Pattern Recognition 44 (2011) 973–987

Contents lists available at ScienceDirect

Pattern Recognition

journal homepage: www.elsevier.com/locate/pr

Gait flow image: A silhouette-based gait representation for human identification

Toby H.W. Lam *, K.H. Cheung, James N.K. Liu

Department of Computing, The Hong Kong Polytechnic University, Hung Hom, Kowloon, Hong Kong

ARTICLE INFO

Article history:
Received 2 June 2010
Received in revised form
7 October 2010
Accepted 11 October 2010

Keywords:
Gait representation
Gait recognition
Gait flow image
Biometrics

ABSTRACT

In this paper, we propose a novel gait representation—gait flow image (GFI) for use in gait recognition. This representation will further improve recognition rates. The basis of GFI is the binary silhouette sequence. GFI is generated by using an optical flow field without constructing any model. The performance of the proposed representation was evaluated and compared with the other representations, such as gait energy image (GEI), experimentally on the USF data set. The USF data set is a public data set in which the image sequences were captured outdoors. The experimental results show that the proposed representation is efficient for human identification. The average recognition rate of GFI is better than that of the other representations in direct matching and dimensional reduction approaches. In the direct matching approach, GFI achieved an average identification rate 42.83%, which is better than GEI by 3.75%. In the dimensional reduction approach, GFI achieved an average identification rate 43.08%, which is better than GEI by 1.5%. The experimental result showed that GFI is stronger in resisting the difference of the carrying condition compared with other gait representations.

1. Introduction

Early medical research has shown that the individual gait, specifically the manner of walking, is unique to each individual and difficult to disguise [1]. It also has been shown that gaits are sufficiently distinctive that people and their gender can be identified by their gait [2,3]. As an identifier of individuals, gait differs from other biometrics such as fingerprints and palm prints, in that it allows a person to be identified at a distance [4]. Further, it requires no contact with any capturing device.

There are two different approaches to gait recognition: model-based and model-free. In model-based gait recognition, information such as joint or hip position is gathered from the body [5–8]. This information is then used to construct a recognition model. In the model-free approach, the gait features are gathered or re-created to become another gait representation from a sequence of binary silhouette images [9–11].

There are a variety of ways to represent a gait. One commonly used method is to use a gait energy image (GEI) [11]; a spatio-temporal gait representation, which is designed to preserve motion information. GEI has also been used in multi-dimensional data analysis [12–15], for gender classification [16,17] and fusion biometrics [18]. GEI represents the recency of the motion; however, it is not embedded with any information of the movement. In our previous work, we proposed two similar gait representations for recognition: Motion silhouette contour template (MSCT), for capturing the motion characteristics of a gait, and static silhouette template (SST) [19] for capturing the static characteristics of a gait. Our experiments showed that the recognition accuracy of MSCT and SST was promising both in indoor and outdoor environments, although they are not yet as accurate as GEI. To further improve the recognition rate, we propose another new data representation, gait flow image (GFI), for gait recognition.

GFI could be computed without the need to construct any model and perform any transformation. We consider each silhouette image as a deformable object. The relative motion information of the gait sequence is determined by using an optical flow field [20]. The optical flow field is the pattern of motion of objects in a scene. The field could be used to perform motion detection, object segmentation and object tracking [21]. In this paper, the optical flow field is adopted to construct the GFI for gait recognition. The advantage of using an optical flow for gait recognition is that it can help to identify the relative motion information. Unlike the approach that extracting a sequence of gait features from each frame of a walking sequence for recognition [22–25], a GFI is extracted in each gait cycle. If the walking sequence has more than one cycle, then a number of GFIs are generated from a walking sequence. This is more computationally efficient, because it obviates the need to generate a sequence of features or perform any transformation.

The efficacy of the proposed representation has been demonstrated on the USF data set [10]. The USF data set contains a number of walking sequences that were constructed from the University of

* Corresponding author.
E-mail address: cshwlam@comp.polyu.edu.hk (T.H.W. Lam).

0031-3203/$ - see front matter © 2010 Elsevier Ltd. All rights reserved.
doi:10.1016/j.patcog.2010.10.011

South Florida in 2001. The walking sequence was captured with a digital camera in an outdoor environment. USF data set is one of the data sets that are commonly used in gait recognition research.

The main contribution of this work is to propose a new gait representation, GFI, to further improve the recognition rate. The experimental results showed that the average recognition rate of the proposed new representation, GFI, has a better performance than GEI, MSCT and SST. In direct matching, GFI achieved an average identification rate 42.83%, which is better than GEI (3.75%), MSCT (8.83%) and SST (13.08%). In the dimensional reduction approach, GFI achieved an average identification rate 43.08% which is better than GEI (1.5%), MSCT (6.0%) and SST (18.08%). These show that GFI is embedded with more distinctive information and more robust compared with other gait representations.

The rest of this paper is organized as follows. Section 2 describes related previous work. Section 3 describes the GFI in detail. Section 4 provides details of the proposed recognition algorithm. Section 5 presents the experimental results. Section 6 offers our conclusion.

2. Previous work

In holistic or model-free approaches, gait recognition utilizes the motion information directly from the silhouette images without the use of a model. Model-free approaches usually use sequences of binary silhouettes which are extracted from a video using segmentation techniques, such as background subtraction. These approaches do require good quality silhouette images to work with.

Little and Boyd adopted an optical flow to develop the shape of motion [26]. The shape of motion is the distribution of the optical flow field. This shape of motion information is then used to determine the phase features and generate a feature vector for recognizing individuals. However, the algorithm is sensitive to noise, such as brightness changes or shadows. Bashir et al. [27] proposed to determine the optical flow from the masked image, where the masked image is the extracted figure-centric image of the walking person by masking. The optical flow field was used to define five different types of motion descriptors. These descriptors were then used for gait recognition. However, the optical flow field depends on the quality of the binary silhouette, which may affect the recognition. Murase and Sakai proposed parametric eigenspace representation for gait recognition and lip reading [23]. The idea is to project the extracted silhouette images onto the eigenspace using principle component analysis (PCA). The sequence of movement forms a trajectory in the eigenspace, namely parametric eigenspace representation. In recognition, the input image sequence is preprocessed to form a sequence of binary silhouettes. This binary sequence is then projected to form a trajectory in the eigenspace. The smallest distance between the input trajectory and the reference trajectory is the best match. The experimental results showed that the parametric eigenspace representation has a potential in gait recognition. Wang and Tan then proposed a new transformation method for reducing the dimensionality of the input feature space by unwrapping a 2D silhouette image and transforming it into a 1D distance signal [25]. The sequence of silhouette images are then transformed to create time-varying distance signals. Similar to Murase and Sakai's work, they apply the eigenspace transformation to the distance signal. Their work showed a promising result on outdoor data. Foster et al. also proposed another time-varying signal for recognition [24]. They proposed an area-based metric called gait masks. Each silhouette in an image sequence is masked, and then the unmasked area is measured. The time-varying signal is formed by using the difference of the unmasked area. The signal acts as a gait signature for recognition. The data size of the time-varying signal depends on the number of frames in the gait sequence. If there is a long gait sequence, the data size of the signal will be large. This is one of the reasons that most of the mentioned research work applied dimensional reduction technique to further reduce the data size.

There is another approach that generates a new gait data representation from the gait sequence for recognition. The major difference between time-varying signal and gait data representation is that the gait representation can greatly reduce the data size, but still retain the distinctive information for recognition. Gait energy image (GEI) [11] is one of the most commonly used data representations in gait recognition. GEI was originally conceptualized by Bobick and Davis's Motion-Energy Image (MEI) and Motion-History Image (MHI) [28]. MEI and MHI are temporal templates. MEI is a binary image which represents where the motion occurred in an image sequence and MHI, which is created from MEIs and is a vector-image where the vector value represents the recency of motion. The major difference between MHI and GEI is that GEI focuses on human walking representation for gait recognition rather than motion recognition. In [19], it was shown that two representations, MSCT and SST, can extract the movement and static informations, respectively. However, the generation of an MSCT mainly used the silhouette contour. Compared with the binary silhouette, the silhouette contour is more sensitive to noise. An SST can only extract the static information from the gait sequence, which is not able to capture the movement information. To compensate for the weaknesses of MSCT and SST, [19] showed how to determine the similarity score from these two representations together for recognition. Liu and Sarkar proposed a similar representation, averaged silhouette, for gait recognition [29]. The silhouette sequence is transformed into a single image representation for use in recognition. Euclidean distance is adopted for similarity measures between these representations. The major problem of the averaged silhouette is that it requires good quality of gait sequences, otherwise, it may affect the recognition rate. To reduce the affect of the silhouette quality, Zhang et al. proposed an active energy image (AEI) [30]. The advantage of AEI is that it can retain the dynamic characteristics of gait for recognition. The active regions are the regions that would be calculated from the difference between two silhouette images in the gait sequence. AEI is created by summing up these active regions. They applied two-dimensional locality preserving projections (2DLPP) for dimension reduction. In their experiments, they showed that an AEI has a higher recognition rate than GEI on the CASIA gait data set [31,32].

3. Gait flow image (GFI)

In this section, we describe the details of the proposed gait recognition algorithm by using gait flow image (GFI). Fig. 1 shows

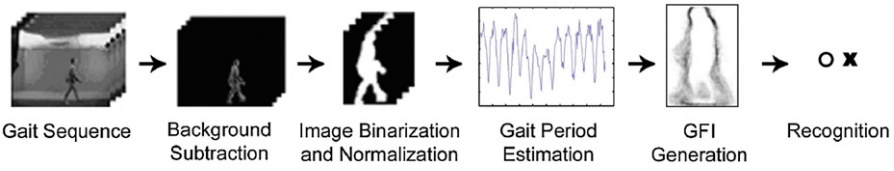

Fig. 1. Flow chart of the proposed recognition algorithm.

the overview of the proposed gait recognition algorithm. The basis of the GFI is the binary silhouettes. The binary silhouettes are extracted from the gait sequence, and then used to determine the gait period. A gait period, or walking cycle, can be seen as a person moving from the mid-stance position to a double support position; subsequently the mid-stance position followed by the double support position and finally back to the mid-stance position. Fig. 2 shows two examples of binary silhouettes within a gait period. After silhouette extraction and gait estimation, the binary silhouettes are arranged to generate the GFI. To determine a GFI, it is necessary to calculate the optical flow field from the gait image sequence. The optical flow field or image velocity field is the pattern of motion of objects in a scene. The GFI would then be used for recognition. The details of each step are shown below.

3.1. Background extraction and image binarization

The main objective of the background extraction is to extract binary silhouettes from the walking sequence. We assume that there is a video camera to capture a gait sequence. The silhouette can be extracted from the gait sequence by using the simple background subtraction, thresholding or the segmentation technique [10,22,25]. Then, the binarization process renders the image in black and white. In general, the background is black (pixel value equals to 0) and the foreground is white (pixel value equals to 1). In this work, we also use this approach to represent the foreground and background informations. The bounding box of the silhouette image is then computed from the binarized image. The silhouette image is cropped according to the position and size of the bounding box. The silhouette is then normalized to a fixed size for an estimation of the gait period. The main purpose of the normalization is to eliminate the scaling effect. For the data sets such as SOTON [33] and CASIA [25,31,32], they provide the binarized images. Therefore, it is necessary to perform normalization before gait period estimation. However, for the USF data set [10], it provides the cropped and normalized silhouette image with the size 128×88. Thus, for the USF data set, it is not necessary to perform any binarization and normalization. In our experiments, the USF data set was used for the evaluation.

3.2. Gait period estimation

The gait period is the number of image frames in each walking cycle. It is necessary to obtain the gait period for the GFI generation process. In most cases, the silhouette contains the smallest number of foreground pixels in the mid-stance position. Similarly, the silhouette contains the greatest number of foreground pixels in the double support position (see Fig. 2). The gait period can be determined by calculating the number of foreground pixels in the silhouette image [10]. However, because sharp changes in the gait cycle are most obvious in the lower part of the body, gait period estimation only makes use of the lower half of the silhouette image. The gait period could be estimated by computing the median of the distance of the three consecutive minima. Fig. 3 shows the variation of the lower half foreground pixels in each frame over time. After we estimated the gait period, the binary silhouettes would further be divided into several cycles according to the estimated gait period, and ready for generating the GFIs.

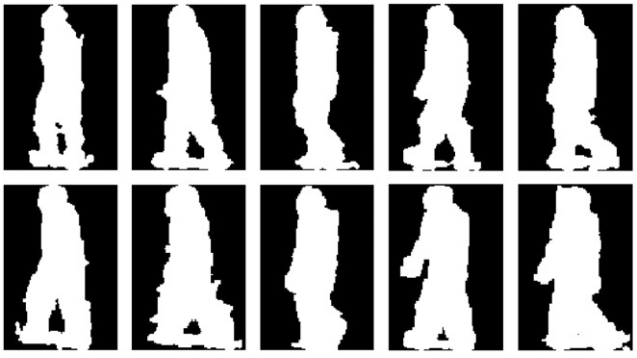

Fig. 2. Samples of silhouettes in a cycle.

3.3. Gait flow image (GFI) generation

A GFI contains the motion information of the human gait. GFIs are generated by determining the optical flow field from the binary silhouettes of each cycle. Two consecutive silhouette images are required to determine an optical flow field. There are two types of optical flow field: the horizontal components of flow $uF_{t,i}$ and vertical components of flow $vF_{t,i}$ (see Fig. 4). We adopted Horn and Schunck's approach to obtain the fields [34] (see Eq. (1)). For the parameter of Horn and Schunck's optical flow, we selected 0.5 as the regularization constant and repeated the computation for five iterations.

$$(uF_{t,\,i}(x,y),\, vF_{t,\,i}(x,y)) = OpticalFlow(SI_{t,\,i}(x,y),\, SI_{t+1,\,i}(x,y)) \tag{1}$$

where $SI_{t,i}(x,y)$ is the silhouette image at time t, t is the time (or the frame number in the gait cycle), i is the cycle number, *OpticalFlow* is Horn and Schunck's optical flow function for calculating the horizontal optical flow field $uF_{t,i}(x,y)$ and vertical optical flow field $vF_{t,i}(x,y)$, and x and y are values in the 2D image coordinate system. These notations t, i, x and y are being applied throughout the paper. The flow fields are then smoothed by Gaussian filter with the filter size 3×3 and standard deviation 0.5. Then, we can obtain the magnitude of $uF_{t,i}$ and $vF_{t,i}$ by Eq. (2).

$$\begin{aligned} MagF_{t,\,i}(x,y) &= ||(uF_{t,\,i}(x,y),\, vF_{t,\,i}(x,y))|| \\ &= \sqrt{(uF_{t,\,i}(x,y))^2 + (vF_{t,\,i}(x,y))^2} \end{aligned} \tag{2}$$

where $MagF_{t,i}(x,y)$ is the resultant magnitude of $uF_{t,i}(x,y)$ and $vF_{t,i}(x,y)$. After this, a binary flow image ($BF_{t,i}$) is generated by Eq. (3). This binary flow image represents the motion of the silhouette images. The dark region means the region with movement. The white region means the region without any movement.

$$BF_{t,\,i}(x,y) = \begin{cases} 0 & \text{if } MagF_{t,\,i}(x,y) \geq 1 \\ 1 & \text{otherwise} \end{cases} \tag{3}$$

where $BF_{t,i}(x,y)$ is the binary flow image at time t in cycle i and $MagF_{t,i}(x,y)$ is the resultant magnitude of $uF_{t,i}(x,y)$ and $vF_{t,i}(x,y)$ at time t in cycle i. The binary flow image is obtained by the simple thresholding

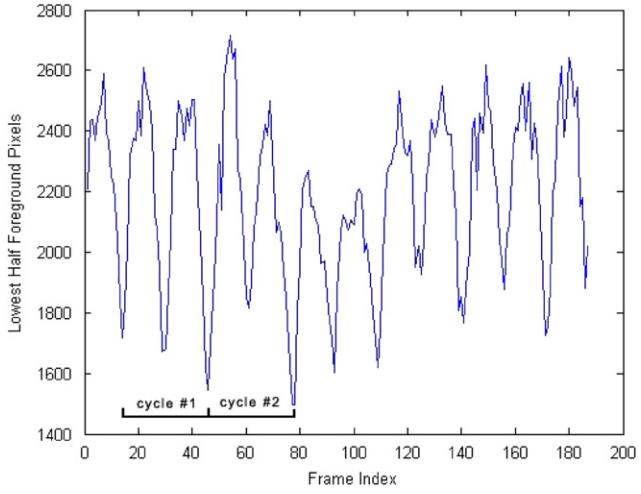

Fig. 3. Variation of the lowest half foreground pixels in each frame over time.

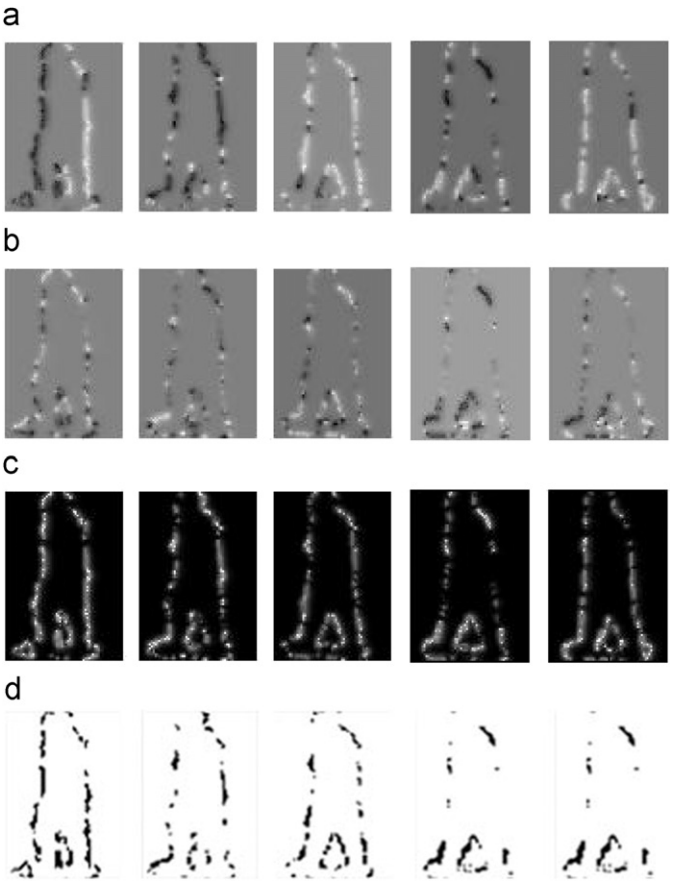

Fig. 4. Optical flow silhouette images: (a) horizontal optical flow field images, (b) vertical optical flow field images, (c) the magnitude of optical flow fields' images and (d) binary flow images.

technique. Since the magnitude value of the optical flows is between 0 and 2, the mid-value, 1, is selected as the threshold value.

In a gait cycle i, if there are N silhouette images, we can generate $N-1$ binary flow images. The GFI can then be created from averaging the binary flow images by using Eq. (4).

$$GFI_i(x,y)=\frac{\sum_{t=1}^{N-1} BF_{t,i}(x,y)}{N} \tag{4}$$

where $BF_{t,i}(x,y)$ is the binary flow image at time t in cycle i and N is the total number of frames in the gait cycle i. Fig. 5 shows some examples of GFI.

The number of GFIs in a sequence depends on the estimated gait period and the number of frames in the walking sequence. In general, subjects have different walking frequencies. Thus, we may get a different number of GFIs for each subject. A great advantage of using GFI is that the number of GFIs is smaller than the number of silhouette images. In other words, GFI is more computationally efficient. However, if the silhouettes are extracted at a low quality, a GFI may be embedded with irrelevant information, which affects the recognition rate. This is the limitation of GFI. Section 4 provides details of the proposed recognition algorithm. These GFIs are used to determine the similarity score for recognition.

3.4. Gait representations for performance comparison

In the experiments, we compared the performance of GFI with other gait representations: gait energy image (GEI), motion silhouette contour template (MSCT) and static silhouette template (SST). As our proposed recognition algorithm is different from their original idea [11,19]; for the sake of completeness of the paper, we include the details of the generation of GEI, MSCT and SST. Similar to the GFI generation process, we assumed that the silhouette images have finished all the pre-processing steps and estimated the gait period.

3.4.1. Gait energy image (GEI)

Suppose the preprocessed binary silhouette image $SI_{t,i}(x,y)$ is extracted at time t in a gait cycle i, gait energy image (GEI) is defined as follows:

$$GEI_i(x,y)=\frac{\sum_{t=1}^{N} SI_{t,i}(x,y)}{N} \tag{5}$$

where N is the number of silhouette images in gait cycle i at time t. Fig. 6 shows some samples of GEI.

3.4.2. Motion silhouette contour template (MSCT)

The MSCT is generated from silhouette contour sequences. At time t in the gait cycle i, the contour of each silhouette image $CSI_{t,i}(x,y)$ is obtained by subtracting the original silhouette $SI_{t,i}(x,y)$ with the eroded silhouette $ESI_{t,i}(x,y)$, as shown in Eq. (6).

$$\begin{aligned} CSI_{t,i}(x,y) &= SI_{t,i}(x,y)-ESI_{t,i}(x,y)=SI_{t,i}(x,y)-(SI_{t,i}(x,y)\times S(x,y)) \\ &= SI_{t,i}(x,y)-\bigcap_{s\in S}(SI_{t,i}(x,y))_{-s} \end{aligned} \tag{6}$$

where $SI_{t,i}(x,y)$ is the original silhouette image, $ESI_{t,i}(x,y)$ is the eroded silhouette, $CSI_{t,i}(x,y)$ is the silhouette contour, S is the structuring element, $\times$ is the eroding operator and $(SI(x,y))_{-s}$ represents the translation of silhouette image $SI_{t,i}(x,y)$ by s, where $s\in S$. The eroded silhouette $ESI_{t,i}(x,y)$ could be computed by an erosion operation. The structuring element S is a set of coordinate points for an erosion operation. Fig. 7 shows the structuring element. The eroding operator is used to superimpose the structuring element with the input image. If each nonzero element of the structuring element is contained in the input image, then the output pixel is white in color (1), otherwise, the output pixel is black in color (0) [35].

Motion silhouette contour template (MSCT) is a gray intensity image, which shows the temporal information. For example, if there is a pixel with a higher pixel value compared with the others, it means that such pixel position has a more recent movement. To retain this temporal information, the intensity decay parameter δ should be computed for each gait sequence. Eq. (7) shows how to determine the value of this parameter.

$$\delta=\frac{255}{N} \tag{7}$$

where N is the total number of frames in the estimated gait period. The use of a dynamic decay value rather than a fixed intensity decay parameter eliminates the walking speed effect. An Eq. (8) is used to create motion silhouette contour template (MSCT) in gait cycle i

$$\begin{aligned} &\text{For } t=1,\ \mathrm{MSCT}_{t,i}(x,y)=CSI_{t,i}(x,y); \\ &\text{For } t>1,\ \mathrm{MSCT}_{t,i}(x,y)=\begin{cases} 255 & \text{if } CSI_{t,i}(x,y)=1 \\ \max(0, MSCT_{t-1,i}(x,y)-\delta) & \text{otherwise} \end{cases} \end{aligned} \tag{8}$$

where δ is the intensity decay parameter, $CSI_{t,i}(x,y)$ is the silhouette contour, $MSCT_{t,i}(x,y)$ is the motion silhouette contour template at time t of gait cycle i and the *max* function is used to prevent negative pixel value. Suppose a gait sequence has N frames, then the final MSCT should be $MSCT_{N,i}(x,y)$. We omit the N notation to represent this final MSCT, i.e. $MSCT_i(x,y)$. This representation will be used for recognition. Fig. 8 shows some examples of MSCT.

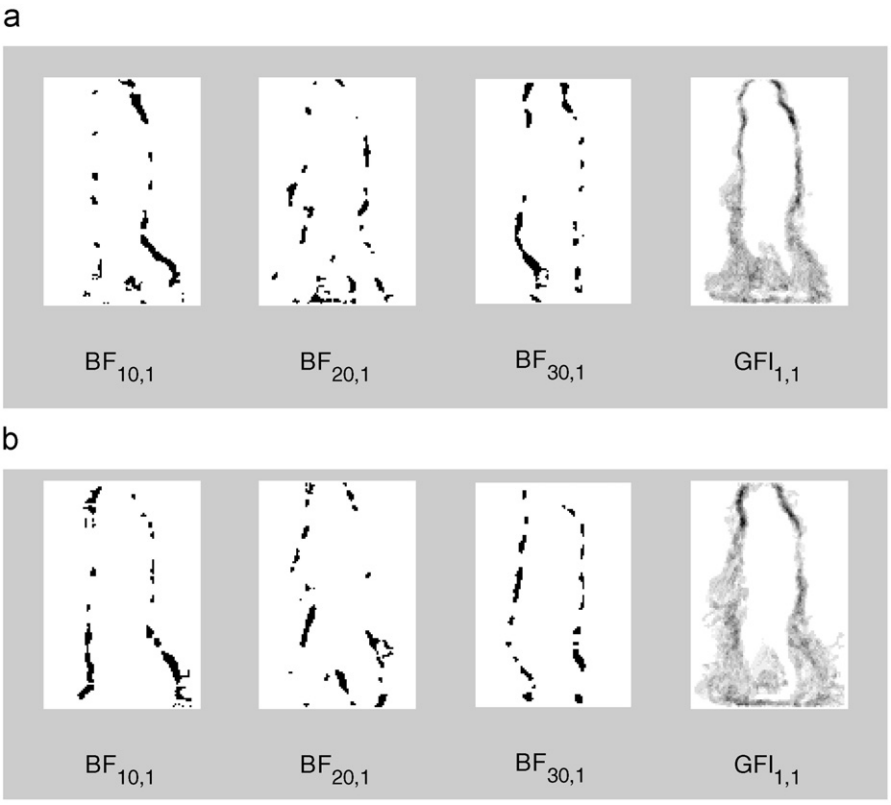

Fig. 5. Examples of gait flow image (GFI) of person (a) 02291 and (b) 03793 in the USF data set.

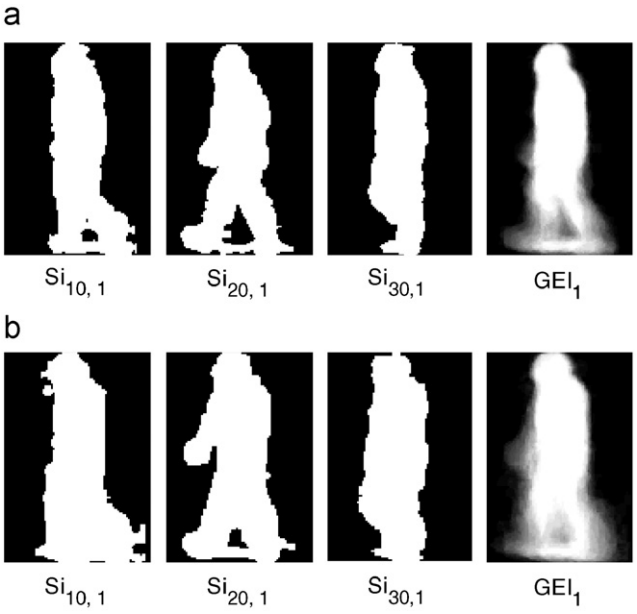

Fig. 6. Examples of gait energy image (GEI) of person (a) 02291 and (b) 03793 in the USF data set.

3.4.3. Static silhouette template (SST)

Static silhouette template (SST) is generated in much the same way as a GEI and MSCT. An SST uses the entire silhouette image and can be generated by using the algorithm (9).

For $t = 1$, $SST_{t,\,i}(x, y) = SI_{t,\,i}(x, y)$;

$$\text{For } t > 1,\ SST_{t,\,i}(x, y) = \begin{cases} 1 & \text{if } SST_{t,\,i}(x, y) = SST_{t-1,\,i}(x, y) \\ 0 & \text{otherwise} \end{cases} \tag{9}$$

1	1	1
1	1	1
1	1	1

Fig. 7. The 3×3 structuring element adopted for an erosion operation.

where $SI_{t,i}(x,y)$ is the silhouette image at time t in cycle i and $SST_{t,i}$ is the static silhouette template at time t in cycle i. Similar to an MSCT, if a gait sequence has an N frame, then the final SST would be written as $SST_i(x,y)$ and this representation will be used for recognition. Fig. 9 shows examples of the SST.

4. Recognition

The similarity score represents the level of similarity between the gallery and the probe data. Suppose there are N subjects in the gallery data set and each subject contains a walking sequence. A similarity score is determined between a gallery sequence and a probe sequence. A gallery sequence $Seq_{gallery} = \{Seq_{gallery}(1), Seq_{gallery}(2), \ldots, Seq_{gallery}(P)\}$ from training data set and a probe sequence $Seq_{probe} = \{Seq_{probe}(1), Seq_{probe}(2), \ldots, Seq_{probe}(Q)\}$ are used for calculating the similarity score, where P and Q are, respectively, the number of gallery and probe sequences. We can obtain P GFIs from the $Seq_{gallery}$. Similarly, for the probe sequence, we can obtain Q GFIs.

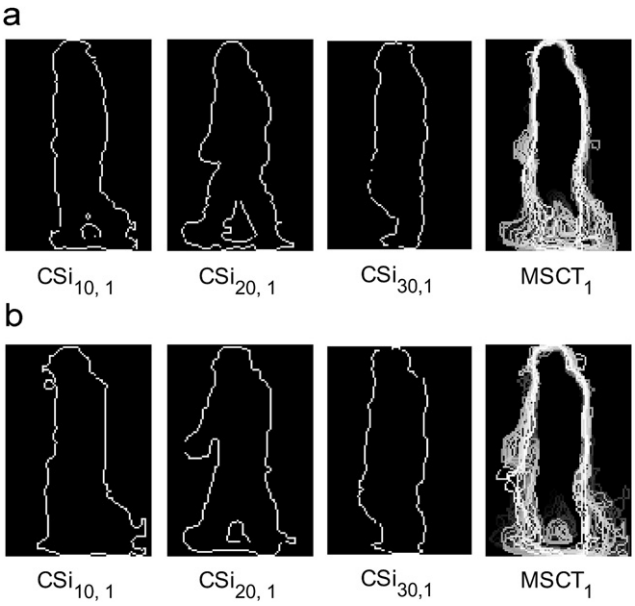

Fig. 8. Examples of motion gait silhouette template (MSCT) of person (a) 02291 and (b) 03793 in the USF data set.

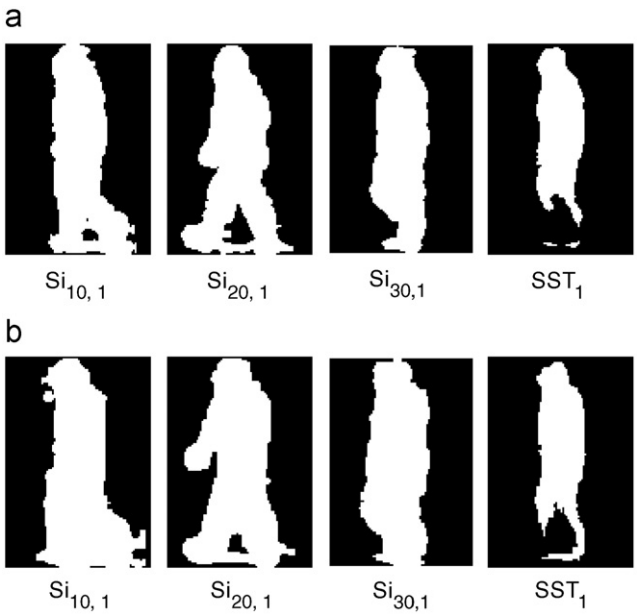

Fig. 9. Examples of silhouette static template (SST) of person (a) 02291 and (b) 03793 in the USF data set.

4.1. Direct matching

To measure the similarity between gallery and probe GFIs, we calculate the similarity score *SimScore*. Since there may be a different number of GFIs in gallery and probe sequences, it may increase the degree of computational complexity during the calculation of the similarity score. To reduce the complexity, an exemplar GFI of each class is obtained. The exemplar GFI is obtained as in Eq. (10).

$$\overline{GFI}_c(x,y)=\frac{\sum_{i=1}^{m} GFI_{c,\,i}(x,y)}{m} \tag{10}$$

where $\overline{GFI}_c(x,y)$ is the exemplar GFI, $GFI_{c,i}(x,y)$ is the GFI of class c in gait cycle i and m is the total number of $GFI_{c,i}$ Fig. 10 shows some examples of an exemplar GFI. The similarity score *SimScore* can be computed by using a normalized Euclidean distance (see Eq. (11)). In our experiments, we adopted an analogous approach to calculate the similarity score for gallery and probe sequence of the GEI, MSCT and SST.

$$SimScore(\overline{GFI}_{gallery}(x,y),\overline{GFI}_{probe}(x,y))=\left\|\frac{\overline{GFI}_{gallery}(x,y)}{\|\overline{GFI}_{gallery}(x,y)\|}-\frac{\overline{GFI}_{probe}(x,y)}{\|\overline{GFI}_{probe}(x,y)\|}\right\| \tag{11}$$

where $\overline{GFI}_{gallery}(x,y)$ is the exemplar gallery GFI and $\overline{GFI}_{probe}(x,y)$ is the exemplar probe GFI.

4.2. Dimension reduction

In the previous section, we described the similarity score calculation for gait recognition in the direct matching approach. However, using this approach makes the dimension relatively large as it depends on the size of the gait representation. We applied linear discriminant analysis (LDA) [36] to reduce the dimensionality. An LDA is a classical dimensionality reduction technique. It is commonly used in biometrics, such as face recognition [36,37] and gait recognition [22,23,25]. The main objective is to transform a high dimension data space into a lower dimension space, but it still retains the most discriminatory information. The details are summarized as follows.

4.2.1. Canonical space transformation

Canonical analysis, or known as linear discriminant analysis, is a dimensional reduction technique. Compared with principle component analysis (PCA) [37], an LDA can overcome the singularity problem. The process of an LDA is as follows:

1. PCA projects the training data to a lower dimensional space with the dimension N–C, where N is the total number of training samples and C is the total number of training classes.
2. Seeking a transformation matrix E_{LDA} with dimension $C-1$ such that it maximizes the ratio of the between-class scatter matrix of the projected samples to the within-class scatter matrix of the projected samples.

PCA is used to capture the principle components of the input space. Suppose there are C classes for training, each class $c \in C$ has N_c of p-dimensional GFI $GFI_{c,i}$, where i is the instance label. The total number of training samples is $N_{total}=N_1+N_2+,\ \ldots,\ +N_c$. The average GFI $\overline{GFI}$ is defined in Eq. (12). From now on, the notation (x, y) is omitted to ease for the presentation.

$$\overline{GFI}=\frac{1}{N_{total}}\sum_{c\in C}\sum_{i=1}^{N_c} GFI_{c,\,i} \tag{12}$$

The average GFI of each class c, $\overline{GFI}_c$ is the same as the exemplar GFI which is defined in Eq. (10). The between-class scatter matrix S_B is defined as

$$S_B=\sum_{c\in C} N_c(\overline{GFI}_c-\overline{GFI})(\overline{GFI}_c-\overline{GFI})^T \tag{13}$$

where N_c is the total number of training sample of class c, $\overline{GFI}_c$ is the average GFI of class c and $\overline{GFI}$ is an average GFI. The within-class scatter matrix S_w is defined as

$$S_w=\sum_{c\in C}\sum_{i=1}^{N_c}(GFI_{c,\,i}-\overline{GFI}_i)(GFI_{c,\,i}-\overline{GFI}_i)^T \tag{14}$$

If S_w has an N rank by using singular value decomposition (SVD), then we can obtain N eigenvalues $\lambda_1, \lambda_2, ..., \lambda_N$ and the associated eigenvectors $e_1, e_2, \ldots, e_N$. Thus, a transformation matrix $E_{PCA}=[e_1, e_2, \ldots, e_q]$ is obtained where $e_1, e_2, \ldots, e_q$ are the eigenvectors corresponding to q largest eigenvalues, where $q<N$. These

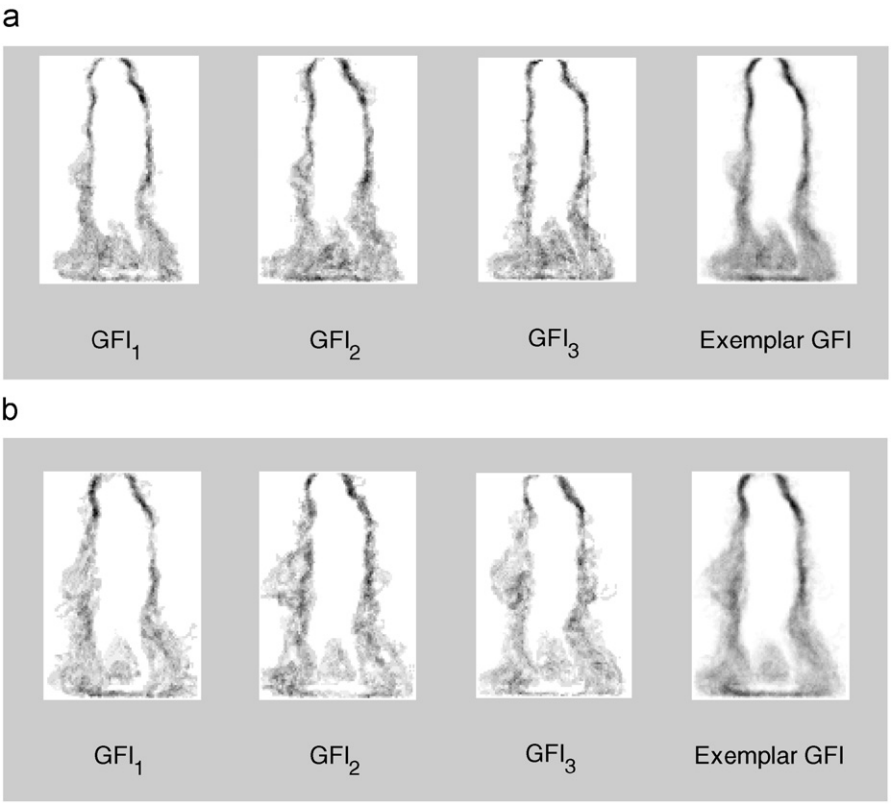

Fig. 10. Examples of exemplar gait flow image (GFI) of person (a) 02291 and (b) 03793 in the USF data set.

eigenvectors are orthonormal to each other and span the eigenspace. For each GFI, $GFI_{c,i}$ is projected to points $s_{c,i}$ in q-dimensional eigenspace by using the eigenspace transformation matrix E_{PCA}.

$$s_{c,\,i} = E_{PCA} GFI_{c,\,i} = [e_1, e_2, \ldots, e_q]^T GFI_{c,\,i} \tag{15}$$

where $c \in C$ and $i = 1, 2, \ldots, N_c$.

In a real situation, PCA introduces the singularity problem. The rank of S_w is at most an $N–C$ [36]. To overcome this problem, $N–C$ eigenvectors are selected and then determine a transformation matrix E_{LDA} to reduce the dimension to $C-1$.

$$E_{LDA} = \arg\max_{E_{LDA}} \frac{\left| E_{LDA}{}^T S_{\tilde{B}} E_{LDA} \right|}{\left| E_{LDA}{}^T S_{\tilde{W}} E_{LDA} \right|} = [g_1, g_2, \ldots, g_{C-1}] \tag{16}$$

where $S_{\tilde{B}}$ is the between-class matrix of the projected training samples and $S_{\tilde{W}}$ is the within-class matrix of the projected training samples and $g_1, g_2, \ldots, g_{C-1}$ are the eigenvectors. For each GFI, $GFI_{c,i}$ is projected to points $s_{c,i}$ in q-dimensional eigenspace by using the eigenspace transformation matrix E_{PCA} first, and then project to points $t_{c,i}$ in $C-1$-dimensional space by using the transformation E_{LDA}.

$$t_{c,\,i} = E_{LDA} s_{c,\,i} = [g_1, g_2, \ldots, g_{C-1}]^T s_{c,\,i} \tag{17}$$

Compared with direct matching approach, there is a slight difference in calculating the similarity score. First, we need to obtain the exemplar probe GFI, $\overline{GFI}_{probe}$(see Eq. (10)). The exemplar probe GFI is projected to lower dimension and obtained the point s_{probe} in $N–C$-dimensional as defined in Eq. (18). Then, the point s_{probe} is further projected to a lower dimensional space by the transformation matrix E_{LDA}. (see Eq. (19)). The similarity score can then be determined by using normalized Euclidian distance between the projected exemplar probe GFI and each projected point of the gallery GFIs $s_{c,i}$ as shown in Eq. (20). A nearest neighbor classifier is adopted for classification (see Section 4.3 for more details).

Table 1
The USF data set.

Probe	Variations	Number of samples
A	View	122
B	Shoe	54
C	View, shoe	54
D	Surface	121
E	Surface, shoe	60
F	Surface, view	121
G	Surface, shoe, view	60
H	Briefcase	120
I	Shoe, briefcase	60
J	View, briefcase	120
K	Time, shoe, clothing	33
L	Surface, time, shoe, clothing	33

$$s_{probe} = E_{PCA} \overline{GFI}_{probe} = [e_1, e_2, \ldots, e_{N-C}]^T \, \overline{GFI}_{probe} \tag{18}$$

$$t_{probe} = E_{LDA} s_{probe} = [g_1, g_2, \ldots, g_{C-1}]^T s_{probe} \tag{19}$$

$$SimScore(t_{probe}, t_{c,i}) = \left\| \frac{t_{probe}}{\|t_{probe}\|} - \frac{t_{c,i}}{\|t_{c,i}\|} \right\| \tag{20}$$

4.3. Classifier

The nearest neighbor classifier is adopted in the proposed recognition algorithm. Suppose there is $N_{gallery}$ training subjects. The testing sample T is classified as class x, if the final score

SimScore, between the projected testing sequence t and training sequence $t_{c,i}$, is the minimum as shown in Eq. (21).

$$x = \min_{i=1}^{N_{gallery}} SimScore(t, t_{c,i}) \quad (21)$$

5. Experiments and results

5.1. USF data set

The proposed new gait representation GFI was tested on the USF data set [10]. We employed the FERET scheme [38], using cumulative match characteristics (CMCs), measured the identification rate and the verification rate. The walking sequence in the USF data set was captured in an outdoor environment. The data set contains 122 subjects and a total of 1870 gait sequences. Compared with other public data sets (e.g. CASIA [25,32,31], SOTON [33]), the USF data set contains a number of subsets offering a range of variables. In the USF data set, there are five different variations—viewpoints, surface, shoe, carrying condition and time. The walking sequences are divided into 13 different subsets: 1 gallery set and 12 probe sets. Table 1 shows details of the USF data set [10]. The performance of the proposed representation was evaluated and compared with the other data representations: gait energy image (GEI) [11], motion silhouette contour template (MSCT) [19] and static silhouette template (SST) [19]. In addition, we also compare the recognition performance with the baseline algorithm [10]. Baseline algorithm is a direct frame

Table 2
Comparison of recognition performance (direct matching).

Probe	Rank 1					Rank 5				
	Baseline (%)	GFI (%)	GEI (%)	MSCT (%)	SST (%)	Baseline (%)	GFI (%)	GEI (%)	MSCT (%)	SST (%)
A	73	*89*	83	67	75	88	*98*	94	91	88
B	78	*93*	89	76	81	93	*94*	*94*	91	89
C	48	70	*74*	54	65	78	*93*	87	80	81
D	*32*	19	19	17	15	*66*	40	46	40	41
E	22	*23*	20	10	17	*55*	47	47	42	33
F	*17*	7	12	6	12	*42*	26	30	21	32
G	*17*	8	15	3	12	*38*	25	35	20	27
H	61	*78*	61	61	28	85	*94*	84	86	57
I	57	*67*	60	60	27	78	*85*	80	*85*	50
J	36	*48*	33	39	16	62	*74*	63	64	32
K	3	3	3	*9*	3	12	*24*	9	21	9
L	3	*9*	0	6	6	15	24	12	*27*	18
Mean	37.25	*42.83*	39.08	34.00	29.75	59.33	*60.33*	56.75	55.67	46.42

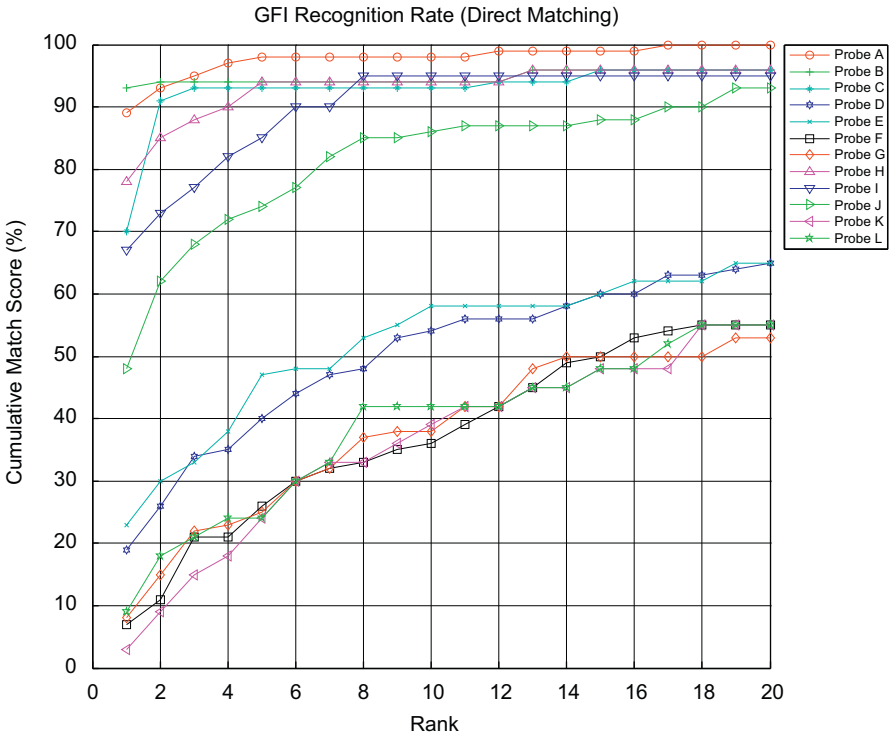

Fig. 11. Recognition rate by using GFI in the USF data set (direct matching).

shape matching approach for gait recognition. Since it is one of the simplest approaches for recognition in the USF data set, this could act as a reference for comparison. All experiments are implemented using Matlab and operated on a Core 2 Quad 2.83 GHz computer with 4 GB memory.

5.2. Performance evaluation in direct matching

Table 2 shows the recognition performance using the direct matching approach. As we adopted a different approach in calculating the similarity score, the identification performance of GEI is

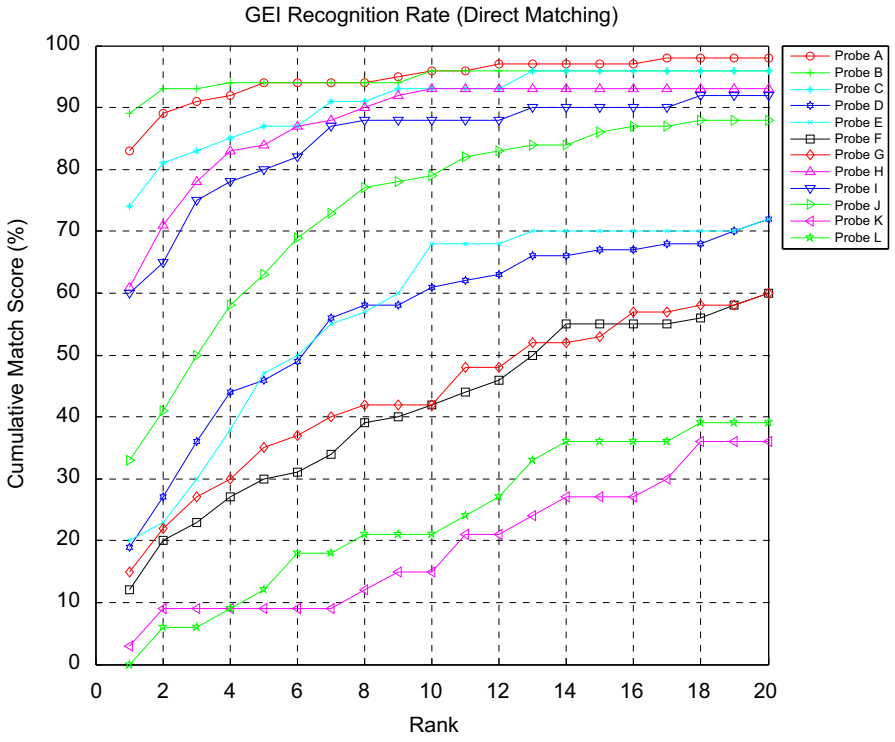

Fig. 12. Recognition rate by using GEI in the USF data set (direct matching).

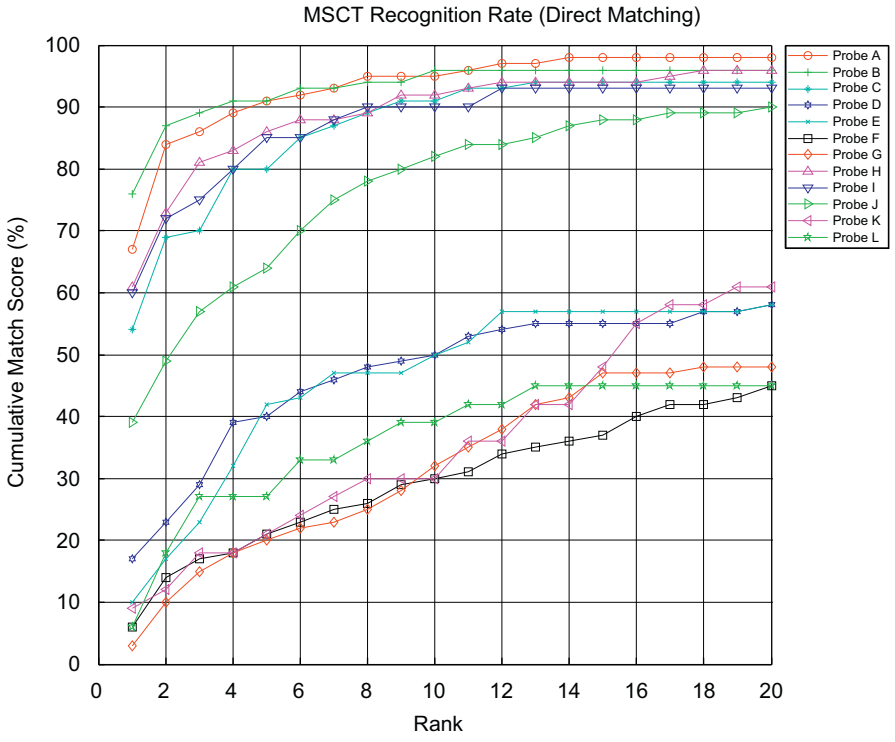

Fig. 13. Recognition rate by using an MSCT in the USF data set (direct matching).

slightly different from [11]. Compared with the others, baseline algorithm has a better recognition performance in Rank 1 in probes D, F and G. It illustrates that the baseline algorithm is strong in resisting different surface conditions. However, GFI has a better overall performance than the other representations. The average identification rate of GFI in Rank 1 is 42.83%. The average identification rate of GEI in Rank 1 is 39.08%, which is 3.75% less than the performance of GFI. GFI has the best identification rate in probes A, B, E, H–J and L. This shows that GFI, in the direct matching approach, retains the discriminative power over the carrying condition and time difference. GEI has the best identification rate in probe C. For the MSCT, it has the best identification rate in probe K. An SST indicates the worst performance when compared with the others. It only has an average identification rate of 29.75%. Figs. 11–14 show the cumulative match score in different ranks under the direct matching approach when using GFI, GEI, MSCT and SST, respectively.

5.3. Performance evaluation in an LDA

The experimental setup was the same as Section 5.2. However, we used an LDA for dimension reduction before classification. In GFI, there are 643 training samples and 122 classes. GEI, MSCT and SST have the same number of training samples and classes. According to Section 4.1, N–C principle components were selected from PCA and the size of dimension was then reduced to $C-1$. Thus, in this experiment, the number of principle components, k, was 521 and the reduced dimension was 121. Table 3 shows the experimental results of the recognition rate by baseline algorithm, GFI, GEI, MSCT and SST.

GFI has the highest average identification rate in Rank 1: 43.08%. The average identification rate of GEI in Rank 1 is 41.58%, which is 1.5% less than the performance of GFI. It shows that the performance of GFI was better than GEI, if we applied an LDA in dimension reduction and selected 521 principle components for

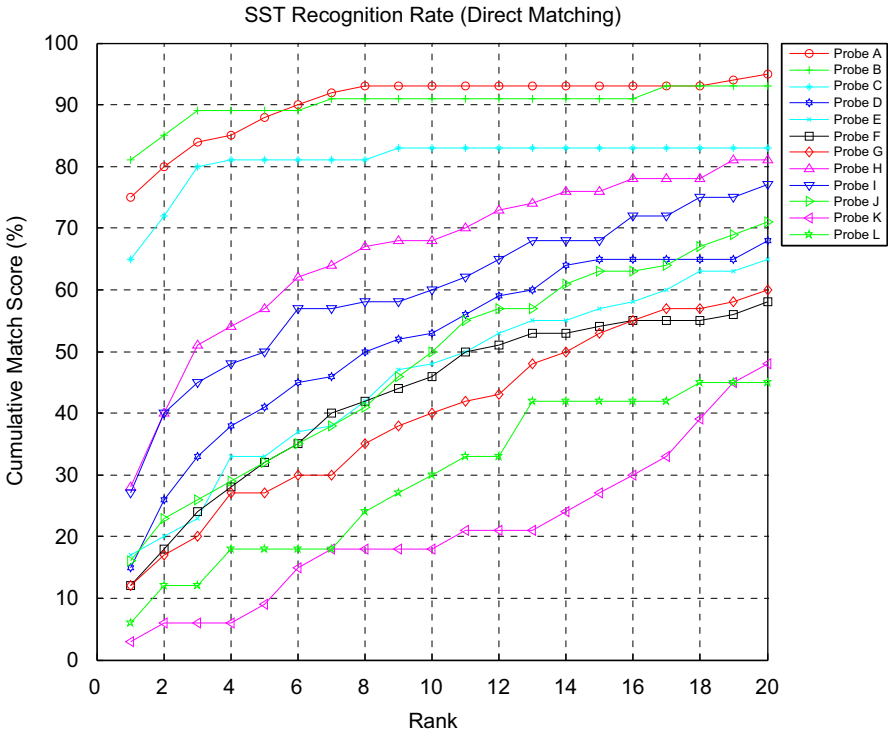

Fig. 14. Recognition rate by using an SST in the USF data set (direct matching).

Table 3
Comparison of recognition performance (LDA, $k=521$).

Probe	Rank 1					Rank 5				
	Baseline (%)	GFI (%)	GEI (%)	MSCT (%)	SST (%)	Baseline (%)	GFI (%)	GEI (%)	MSCT (%)	SST (%)
A	73	82	*87*	77	69	88	*89*	*89*	84	80
B	78	89	*91*	81	74	*93*	91	91	89	85
C	48	*76*	*76*	59	52	78	*80*	*80*	74	57
D	*32*	27	26	24	14	*66*	37	34	36	25
E	22	*27*	22	20	13	*55*	32	28	30	20
F	*17*	10	10	12	6	*42*	16	15	18	8
G	*17*	*17*	15	7	3	*38*	28	25	8	10
H	*61*	60	47	52	19	*85*	67	55	60	22
I	*57*	*57*	52	52	17	*78*	67	60	58	22
J	36	*54*	58	43	18	62	*73*	68	56	31
K	3	*15*	9	12	9	12	*18*	12	18	12
L	3	3	*6*	*6*	*6*	*15*	9	9	9	9
Mean	37.25	*43.08*	41.58	37.08	25.00	*59.33*	50.58	47.17	45.00	31.75

recognition. Figs. 15–18 give the cumulative match score in different ranks, under an LDA approach with $k=521$, by using GFI, GEI, MSCT and SST, respectively. GFI has the same identification rate as the baseline algorithm in probes G and I. In addition, GFI has an identification rate very close to that of baseline in probe H (GFI: 60%; baseline: 61%). GEI has the best identification rate in probes A, B, J and L. MSCT and SST have the same identification rate as GEI in probe L.

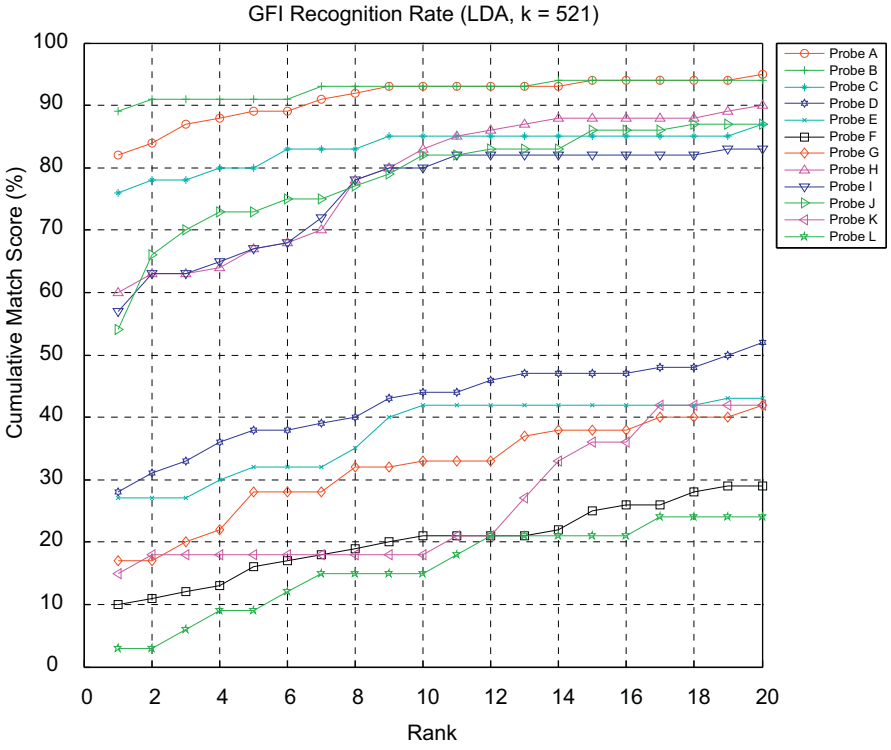

Fig. 15. Recognition rate by using GFI in the USF data set (LDA with $k=521$).

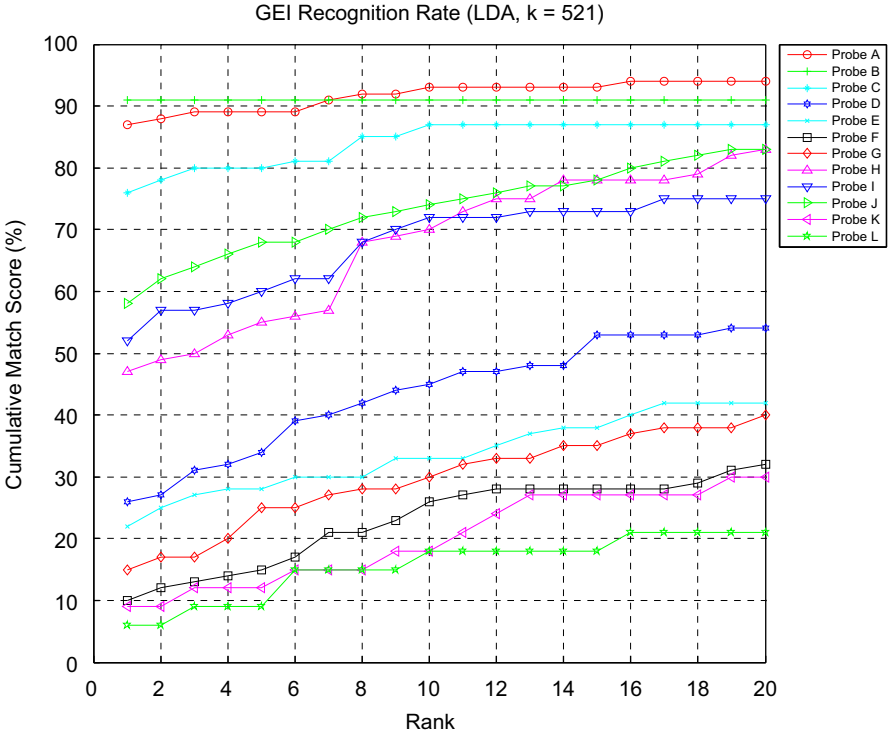

Fig. 16. Recognition rate by using GEI in the USF data set (LDA with $k=521$).

5.3.1. Performance evaluation in different number of principle components

We further explored the recognition rate with respect to the different number of principle components k. As if the k is less than C or k is too large, the Sw matrix becomes uninvertible. Thus, we defined the range of k between 512 (N–C) and 244 ($2C$) in this experiment. Then, we repeated the previous experiment with 500 principle components, decreasing the number in steps of 50, until it reached 250. Then, we repeated the experiments again with the maximum ($k=521$) and minimum ($k=244$) number of principle components. Fig. 19 shows the recognition rate with different number of principle components k. This shows that GEI has a better

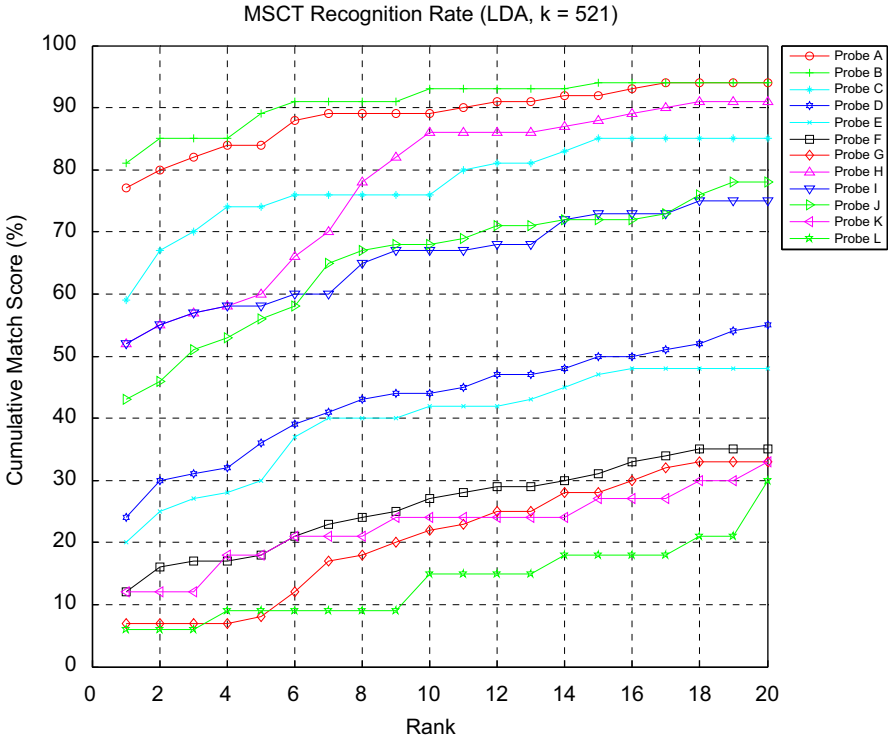

Fig. 17. Recognition rate by using an MSCT in the USF data set (LDA with $k=521$).

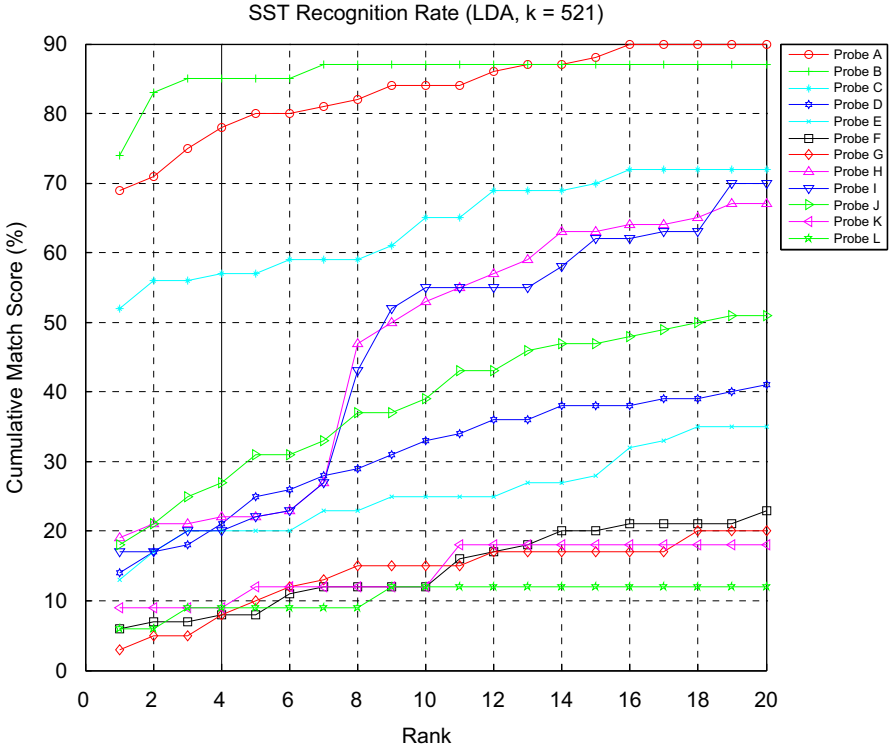

Fig. 18. Recognition rate by using an SST in the USF data set (LDA with $k=521$).

performance than GFI in probes A and B, when k is greater than 300. When k is less than or equal to 300, GFI has a better performance GEI in probes A and B. Fig. 19 also shows that GFI has a consistently high recognition in probes H and I. Thus, compared with the other gait representations, GFI strongly resists the carrying condition. Table 4 shows the average recognition with different number of principle components k. GFI has a better performance than GEI, MSCT and SST, except $k=400$. GFI has the best recognition rate of 44.83% when there are 300 principle components.

5.4. Discussion

From the experimental results shown in Tables 2 and 3, they illustrated that GEI is strong in resisting view and shoe differences and GFI is strong in resisting the carrying condition. GFI can achieve a high recognition rate in probes E, H and I after an LDA ($k=521$). This shows that GFI, after dimension reduction, can still retain the discriminative features in carrying condition for gait recognition. To examine the properties of GFI in gait recognition, we selected a number of the principle components (eigenvectors) from GFIs and re-constructed them to be in 2D representations, namely eigenflows, for further analysis. In Fig. 20, the first eight eigenflows are shown. Fig. 20(a) and (b) corresponds to the largest and the second largest eigenvalues, respectively, and so on. The first eigenflow captures most of the energy in the upper front and back of the body and the second eigenflow capture most of the energy in the back region of the head. By observation, the eigenflows reserve the silhouette contour and the central area of the eigenflows, which is similar to the static silhouette template (SST). The critical regions of GFI fall into the upper and back regions of the head. This showed that the proposed GFI gait representation mainly utilizes the upper and back regions of the head for gait recognition. Since it has not contained much energy in the hand regions, this is one of the reasons that GFI is strong in resisting the carrying condition.

6. Conclusion

In this paper, we have proposed a new data representation, gait flow image (GFI), for gait recognition. The performance of the GFI was evaluated experimentally using the USF data set. The performance of GFI is better than GEI, MSCT and SST in the direct matching and LDA approaches. The best average recognition rate of GFI is 44.83% when k is equal to 300, where GEI has 39.67%, MSCT

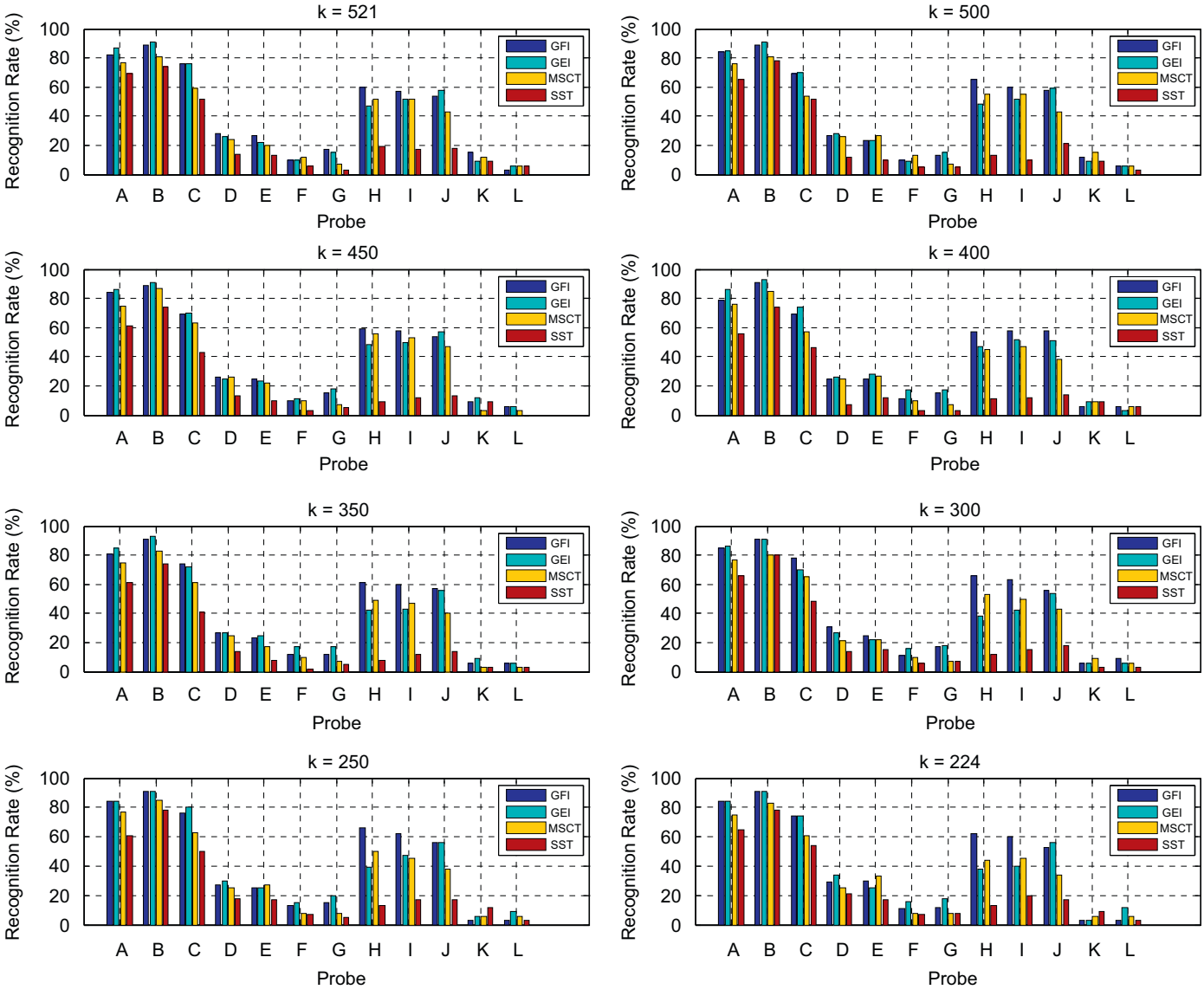

Fig. 19. Recognition rate with different number of principle components k in LDA.

Table 4
The average recognition rate with different number of principle components k in LDA.

Average recognition rate	Number of principle components k							
	521	**500**	**450**	**400**	**350**	**300**	**250**	**244**
GFI (%)	43.08	42.92	41.91	41.58	42.41	*44.83*	43.33	42.5
GEI (%)	41.58	41.25	41.42	*41.92*	41	39.67	41.83	40.92
MSCT (%)	37.08	*38.17*	37.67	36	35	36.92	36.5	35.67
SST (%)	25.00	23.58	21	21.08	20.42	23.92	24.83	*26*

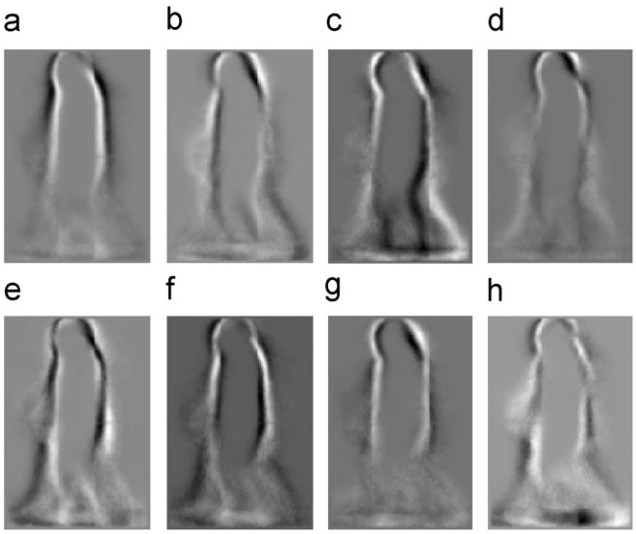

Fig. 20. Eigenflows corresponding to the eight largest eigenvalues.

has 36.92% and an SST has 23.92%. When $k=300$, GFI has the best recognition rate in the USF data set. To conclude, the performance of the proposed GFI representation is comparable to GEI. However, similar to GEI and the other silhouette-based representations, there is a limitation that the silhouettes lose some discriminative walking information, due to the quality of the extracted silhouettes. Recently, a public data set has become available, CASIA data set C, i.e. a data set for gait recognition at night [31]. This data set contains the gait sequence captured outdoors at night, using thermal infrared cameras. The silhouette image is more noise-free. It was shown that the silhouettes from [31,39] captured by an infrared thermal camera, could improve the quality of the extracted silhouettes. In the future, we would like to verify the performance of the proposed representation in the night gait recognition and seek a new feature extraction scheme to further improve the recognition. Furthermore, we would like to investigate the recognition rate if the dynamic thresholding is adopted during binary flow image construction and develop a hardware, which could be attached to the human body for use in capturing gait features for recognition.

References

[1] M. Murray, A. Drought, R. Kory, Walking patterns of normal men, Journal of Bone and Joint Surgery 46 (2) (1964) 335–360.
[2] C.D. Barclay, J.E. Cutting, L.T. Kozlowski, Temporal and spatial factors in gait perception that influence gender recognition, Perception and Psychophysics 23 (2) (1978) 145–152.
[3] J. Cutting, L. Kozlowski, Recognizing friends by their walk: gait perception without familiarity cues, Bulletin of the Psychonomic Society 9 (5) (1977) 353–356.
[4] A.K. Jain, S.Z. Li, in: Encyclopedia of Biometrics, Springer, 2009.
[5] C.Y. Yam, M.S. Nixon, J.N. Carter, Automated person recognition by walking and running via model-based approaches, Pattern Recognition 37 (5) (2004) 1057–1072.
[6] D.K. Wagg, M.S. Nixon, On automated model-based extraction and analysis of gait, in: *Proceedings of the Sixth IEEE International Conference Automatic Face and Gesture Recognition*. (2004) 11–16.
[7] A.F. Bobick, A.Y. Johnso, Gait recognition using static, activity-specific parameters, in: *Proceedings of the IEEE Computer Vision and Pattern Recognition Conference*. (2001) 423–430.
[8] L. Wang, H. Ning, T. Tan, W. Hu, "Fusion of static and dynamic body biometrics for gait recognition, IEEE Transactions on Circuits and Systems for Video Technology 14 (2) (2004) 149–158.
[9] A. Kale, et al., "Identification of humans using gait, IEEE Transactions on Image Processing 13 (9) (2004) 1163–1173.
[10] S. Sarkar, P.J. Phillips, Z. Liu, I.R. Vega, P. Grother, K.W. Bowyer, The humanID gait challenge problem: data sets, performance, and analysis, IEEE Transactions on Pattern Analysis and Machine Intelligence 27 (2) (2005) 162–177.
[11] J. Han, B. Bhanu, Individual recognition using gait energy image, IEEE Transactions on Pattern Analysis and Machine Intelligence 28 (2) (2006) 316–322.
[12] D. Tao, X. Li, X. Wu, S. Maybank, General tensor discriminant analysis and Gabor features for gait recognition, IEEE Transactions on Pattern Analysis and Machine Intelligence 29 (10) (2007) 1700–1715.
[13] H. Lu, K.N. Plataniotis, A.N. Venetsanopoulos, MPCA: multilinear principal component analysis of tensor objects, IEEE Transactions on Neural Networks 19 (1) (2008) 18–39.
[14] D. Xu, S. Yan, D. Tao, S. Lin, H. Zhang, Marginal Fisher analysis and its variants for human gait recognition and content-based image retrieval, IEEE Transactions on Image Processing 16 (11) (2007) 2811–2821.
[15] X. Li, S. Lin, S. Yan, D. Xu, Discriminant locally linear embedding with high-order tensor data, IEEE Transactions on Systems, Man, and Cybernetics, Part B (Cybernetics) 38 (2) (2008) 342–352.
[16] X. Li, S. Maybank, S. Yan, D. Tao, D. Xu, Gait components and their application to gender recognition, IEEE Transactions on Systems, Man, and Cybernetics, Part C (Applications and Reviews) 38 (2) (2008) 145–155.
[17] S. Yu, T. Tan, K. Huang, K. Jia, X. Wu, A study on gait-based gender classification, IEEE Transactions on Image Processing 18 (8) (2009) 1905–1910.
[18] X. Zhou, B. Bhanu, Feature fusion of side face and gait for video-based human identification, Pattern Recognition 41 (3) (2008) 778–795.
[19] T. Lam, R. Lee, D. Zhang, Human gait recognition by the fusion of motion and static spatio-temporal templates, Pattern Recognition 40 (9) (2007) 2563–2573.
[20] S.S. Beauchemin, J.L. Barron, The computation of optical flow, ACM Computing Surveys (CSUR) 27 (3) (1995) 466.
[21] A. Yilmaz, O. Javed, M. Shah, Object tracking: a survey, ACM Computing Surveys 38 (4) (2006) 13.
[22] P.S. Huang, C.J. Harris, M.S. Nixon, Human gait recognition in canonical space using temporal templates, IEE Proceedings—Vision, Image, and Signal Processing 146 (2) (1999) 93.
[23] H. Murase, R. Sakai, Moving object recognition in eigenspace representation: gait analysis and lip reading, Pattern Recognition Letters 17 (2) (1996) 155–162.
[24] J.P. Foster, M.S. Nixon, A. Prügel-Bennett, Automatic gait recognition using area-based metrics, Pattern Recognition Letters 24 (14) (2003) 2489–2497.
[25] L. Wang, T. Tan, H. Ning, W. Hu, Silhouette analysis-based gait recognition for human identification, IEEE Transactions on Pattern Analysis and Machine Intelligence 25 (12) (2003) 1505–1518.
[26] J. Little, J. Boyd, Recognizing people by their gait: the shape of motion, Videre, Journal of Computer Vision Research 1 (2) (1998) 1–32.
[27] K. Bashir, T. Xiang, S. Gong, Gait representation using flow fields, Proceedings of the British Machine Vision Conference 2009 (2009).
[28] A.F. Bobick, J.W. Davis, The recognition of human movement using temporal templates, IEEE Transactions on Pattern Analysis and Machine Intelligence 23 (3) (2001) 257–267.
[29] Z. Liu, S. Sarkar, Simplest representation yet for gait recognition: averaged silhouette, Proceedings of the ICPR 4 (2004) 211–214.
[30] E. Zhang, Y. Zhao, W. Xiong, Active energy image plus 2DLPP for gait recognition, Signal Processing 90 (7) (2010) 2295–2302.
[31] D. Tan, K. Huang, S. Yu, T. Tan, Efficient night gait recognition based on template matching, Proceedings of the 18th International Conference on Pattern Recognition (ICPR) 3 (2006) 1000–1003.

[32] S. Yu, D. Tan, T. Tan, A framework for evaluating the effect of view angle, clothing and carrying condition on gait recognition, Proceedings of the 18th International Conference on Pattern Recognition (ICPR) 4 (2006) 441–444.
[33] J. Shutler, M. Grant, M. Nixon, J. Carter, On a large sequence-based human gait database, Proceedings of the 4th International Conference on Recent Advances in Soft Computing (RASC) (2002) 66–72.
[34] B.K. Horn, B.G. Schunck, Determining optical flow, Artificial Intelligence 17 (1981) 185–203.
[35] R. van den Boomgaard, R. van Balen, Methods for fast morphological image transforms using bitmapped binary images, CVGIP: Graphical Models and Image Processing 54 (3) (1992) 252–258.
[36] P. Hespanha, D.J. Kriegman, Eigenfaces vs. Fisherfaces: recognition using class specific linear projection, IEEE Transactions on Pattern Analysis and Machine Intelligence 19 (7) (1997) 711.
[37] M. Turk, A. Pentland, Eigenfaces for recognition, Journal of Cognitive Neuroscience 3 (1) (1991) 71–86.
[38] P.J. Phillips, H. Moon, S.A. Rizvi, P.J. Rauss, The FERET evaluation methodology for face-recognition algorithms, IEEE Transactions on Pattern Analysis and Machine Intelligence 22 (10) (2000) 1090–1104.
[39] Z. Xue, D. Ming, W. Song, B. Wan, S. Jin, Infrared gait recognition based on wavelet transform and support vector machine, Pattern Recognition 43 (8) (2010) 2904–2910.

Toby H.W. Lam received his B.Sc. (Hons.) and Ph.D. degrees in Department of Computing from The Hong Kong Polytechnic University, Hong Kong, in 2003 and 2007, respectively. Currently, he is a Teaching Fellow in Department of Computing, The Hong Kong Polytechnic University. His major research areas include: gait recognition, pattern recognition and biometrics.

King Hong Cheung received his B.A. (Hons.) degree in Computing from The Hong Kong Polytechnic University, Hong Kong, in 1999 and he received his Ph.D. from the same university in 2006. He is now working as a Teaching Fellow in Department of Computing, The Hong Kong Polytechnic University. His research interests include biometrics, pattern recognition, image processing and retrieval.

James N.K. Liu received the B.Sc. (Hons.) and M.Phil. degrees in mathematics and computational modeling from the Murdoch University, Perth, Australia, in 1982 and 1987, respectively. He received his Ph.D. Degree in artificial intelligence from the La Trobe University, Melbourne, Australia, in 1992. While working on his degree, he worked as a computer scientist at Defence Signal Directorate in Australia from 1988 to 1990. He joined the Aeronautical Research Laboratory (ARL) of Defence Science and Technology Organization in Australia as a research scientist in 1990. At ARL, he helped perform AI research in areas of human factors and mission enhancement.

Dr. Liu joined The Hong Kong Polytechnic University, as a faculty member in 1994, and currently holds the position of Associate Professor in the Department of Computing. He has published technical papers on subjects in pattern recognition, biometrics technology, expert system verification, forecasting systems and e-Commerce applications. His current interests include pattern recognition, ontology-based agent systems, intelligent business computing, forecasting applications and data mining. He is a senior member of IEEE and a member of AAAI.